Chemical Engineering Journal 476 (2023) 146727

Contents lists available at ScienceDirect

Chemical Engineering Journal

journal homepage: www.elsevier.com/locate/cej

Resilient photoswitchable metal–organic frameworks for sunlight-induced on-demand photochromism in the solid state

Samraj Mollick [a], Yang Zhang [a], Waqas Kamal [b], Michele Tricarico [a], Annika F. Möslein [a], Vishal Kachwal [a], Nader Amin [c], Alfonso A. Castrejón-Pita [b], Stephen M. Morris [b], Jin-Chong Tan [a,*]

[a] Multifunctional Materials & Composites (MMC) Laboratory, Department of Engineering Science, University of Oxford, Parks Road, Oxford OX1 3PJ, United Kingdom
[b] Department of Engineering Science, University of Oxford, Parks Road, Oxford OX1 3PJ, United Kingdom
[c] Department of Chemistry, University of Oxford, Mansfield Road, Oxford OX1 3TA, United Kingdom

ARTICLE INFO

Keywords:
Metal-organic frameworks (MOFs)
Nanocomposites
Solid state photochromism
Film
Photostable
Mechanical property

ABSTRACT

Organic photoswitchable molecules have struggled in solid-state form to fulfill their remarkable potential, in terms of photoswitching performance and long-term stability when compared to their inorganic counterparts. We report the concept of non-electron deficient host's surface with optimal porosity and hydrophobicity, as *a priori* strategy to design photoefficient organic solid-state photochromic materials with outstanding mechanical robustness. It is realized by the nanoconfinement of photochromes in a host matrix possessing optimal porosity and hydrophobicity. The resulting photochromic nanocomposites can be prepared in multigram scale employing a one-pot reaction under ambient conditions. When exposed to a light stimulus including natural sunlight, the photoswitchable nanocomposite powder changes color promptly and reversibly, in a matter of seconds (5 s and 30 s under UV irradiation and sunlight, respectively) along with excellent photo-fatigue resistance, which are on a par with inorganic photochromes. Exemplars of commercially viable prototypes that are optically clear, comprising smart windows, complex photochromic sculptures, and self-erasing rewritable devices, were engineered by direct blending with resilient polymers. Notably, the use of high-stiffness polymers (Young's modulus > 2 GPa) is no longer considered an insurmountable challenge. Finally, photochromic films with anticounterfeiting features could be manufactured through precision printing of nanocrystals by drop-on-demand inkjet printing technology.

1. Introduction

Inspired by nature's large repertoire of biological processes, scientists have developed stimuli-responsive smart systems constructed from unique photochromic switches that can reversibly change color; this field has recently attracted considerable scientific interest [1–7]. Conversion of such photochromic molecules into continuum materials will enable translation of stimuli-controlled nanoscopic changes to the macroscopic scale [8–12]. In 1964, Corning (USA) marketed the first photochromic ophthalmic lenses based on silver halide crystals [13], and ever since, photochromism has been exploited to evolve into a global multimillion-dollar industry [14]. Despite their prevalence in scientific research publications, organic photochromic materials have appeared far less in commercial applications although the field is growing in the industrial sector. For example, spiropyran (SP) molecules are amongst the most versatile organic photochromic materials, whose geometry transforms from a closed-ring (nonpolar) form to an opened-ring (highly polar merocyanine) form upon exposure to ultraviolet (UV) light, while the reverse process can be triggered by visible light as well as by a variety of other stimuli [15–20]. This intriguing reversible visual color-switching ability provides numerous opportunities for a variety of different fields, such as optoelectronic devices, data storage, fiber optics, bioadhesive mediators, optical delay generators, and much more [21–24]. However, the low efficiency and poor long-term stability of such multifunctional SP molecules in the solid state have hindered their commercial and industrial proliferations [14,25,26]. Recently, encapsulation into a confined microenvironment of a porous solid state material has been recognized as an effective strategy to markedly

* Corresponding author.
E-mail address: jin-chong.tan@eng.ox.ac.uk (J.-C. Tan).

https://doi.org/10.1016/j.cej.2023.146727
Received 4 August 2023; Received in revised form 30 September 2023; Accepted 15 October 2023
Available online 17 October 2023

improve the chemical and physical properties of organic photoswitchable molecules [27–32]. Nevertheless, the photoisomerization process of such solid-state photoswitchable materials has specific challenges, and this significantly hampers their capability due to geometrical constraints imposed by the solid state environment [33,34]. To this end, the primary endeavor in the current research is to accomplish efficient bulk photoresponsivity integrated in a robust solid matrix of nanoporous materials, without compromising the remarkable molecular photoisomerization properties.

Metal-organic frameworks (MOFs) have recently become a considerable hot topic for photoresponsive applications, owing to their vastly tunable properties and porosity by design [35–40]. Photoresponsive MOFs are primarily tailored for light modulated guest separation/storage and conductivity applications [41–44], and increasingly for guest-induced luminescent sensing [45]. Despite the fact that multiple attempts have been made to improve the overall performance efficiency and durability of photoswitchable SP molecules through encapsulation inside the MOF cavity, the majority have suffered from a lack of intense color changing features which are critical for real-world applications [34,46]. Moreover, the majority of the porous photochromic materials are insensitive to sunlight due to their low photochromic performance efficiency [47,48]. Additionally, none of them satisfies or is nowhere close to the inorganic commercial photochromic materials in terms of both performance and long-term stability. Hence, a rational design strategy for the selection of suitable MOF hosts is urgently needed for sunlight-induced photochromism to meet the commercial/industrial standards set for photochromic materials, but this has remained elusive.

In this study, we have judiciously engineered and harnessed the microenvironment of a series of MOFs, where non electron deficient surface with intermediate hydrophobicity and optimal porosity offers efficient solid state photoswitchable materials. The newly designed photochromic fluorescent nanocomposites were systematically characterized by a wide range of spectroscopic techniques to gain insights into the materials in the bulk powder phase, as single crystals, membranes and thin films. We demonstrate that intense color switching, outstanding long-term stability, enhanced photo-fatigue resistance, production scalability, along with efficient solution-like photochromic response in the solid state are achievable using the proposed approach. Specifically, we show that the optimal porosity provides enough room for the geometrical transformation of the photochromic guest confined in the MOF pore, while intermediate hydrophobicity enables fast reversible switching and enhanced stability. Additionally, we have fabricated commercial grade photochromic prototypes, for instance, high-quality films, 3-D sculptures with complex geometries, smart windows and self-erasing rewritable screens, using a mechanically stiff polymer such as polystyrene (Young's modulus, E ~ 4 GPa). Hitherto, this was unattainable, due to poor performance when photoswitchable molecules are combined with rigid polymers. Finally, to mimic practical applications, alongside an assortment of prototype photochromic sculptures, self-erasing rewritable surfaces, bare photochromic materials were inkjet printed at the nanometer scale on a wide range of technical substrates for fabricating thin-film photoswitchable devices.

2. Results

2.1. Design of efficient photochromic solids

We have identified three photochromes: spiropyran (SP), nitro

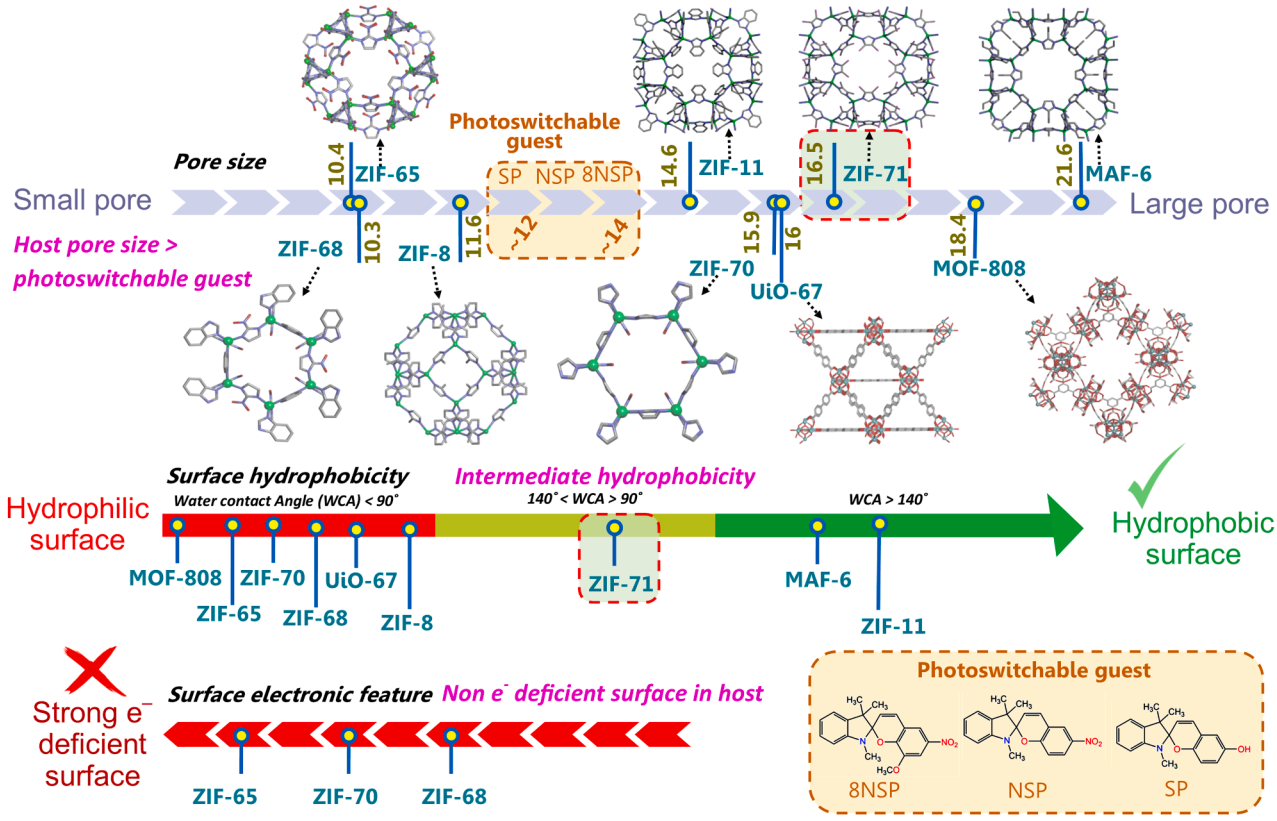

Fig. 1. Schematic illustration of a general design strategy comprising of pore size, surface hydrophobicity and surface electronic feature for high-performance photochromic materials. Different prototype MOFs were used as host matrices for the encapsulation of organic photochromic spiropyran guest molecules. Here, porous frameworks with a cavity size larger than the spiropyran guest are classified as 'large pore', while frameworks with a pore cavity smaller than the spiropyran guest are termed as 'small pore'. Three different organic photochromic guests coined as SP, NSP and 8NSP.

spiropyran (NSP), and 8–methoxy nitrospiropyran (8NSP) as promising spiropyran molecules for the organic photochromic guest. A variety of MOF structures with different topologies and surface features was screened as a host matrix, in accordance with the selection rules depicted in Fig. 1, giving the best performing photoisomerization of the encapsulated guest (Figs. S1–S8 and Table S1). In this work, UiO-67 and MOF-808, UiO-67 and ZIF-8 for hydrophilic pore surface; ZIF-65, ZIF-68 and ZIF-70 for nitro-functional group containing pore surface; ZIF-71, MAF-6 and ZIF-11 for hydrophobic pore surface, were interrogated as a prototypal host matrix to construct photochromic guest@MOF composites (Fig. 1). The photochromic composites with various ZIF hosts, including ZIF-8, ZIF-11, ZIF-65, ZIF-71, and MAF-6, were fabricated at room temperature using a straightforward single-step in situ confinement methodology. Photochromic composites with other hosts such as ZIF-68, ZIF-70, UiO-67, and MOF-808 were synthesised at high temperatures using solvothermal reaction conditions (see SI for more details).

We have proposed a generic design strategy for the identification of an appropriate host matrix for development of efficient solid-state photochromism. When the pore size of a MOF, specifically ZIF-11 with a pore size of 14.6 Å, is in close proximity to the size of the open-form guest molecule, the performance of the transformation from a closed to open form is hindered. Conversely, when the pore size is markedly larger, such as in MAF-6 with a pore size of 21.6 Å, the transformation efficacy is reduced. However, when the pore size of a framework, such as ZIF-71 with a pore size of 16.5 Å, is intermediate in size, the transformation performance from a closed to open form is notably enhanced (Fig. 1). In this case, with an optimal pore size, i.e., pore size ≥ open size of the guest (Scheme S1), this configuration will facilitate the easy switching of the guest molecule from closed to open form. Similarly, the ring-opening process of NSP is significantly impeded when the hydrophobicity of the host frameworks is considerably increased, as evidenced

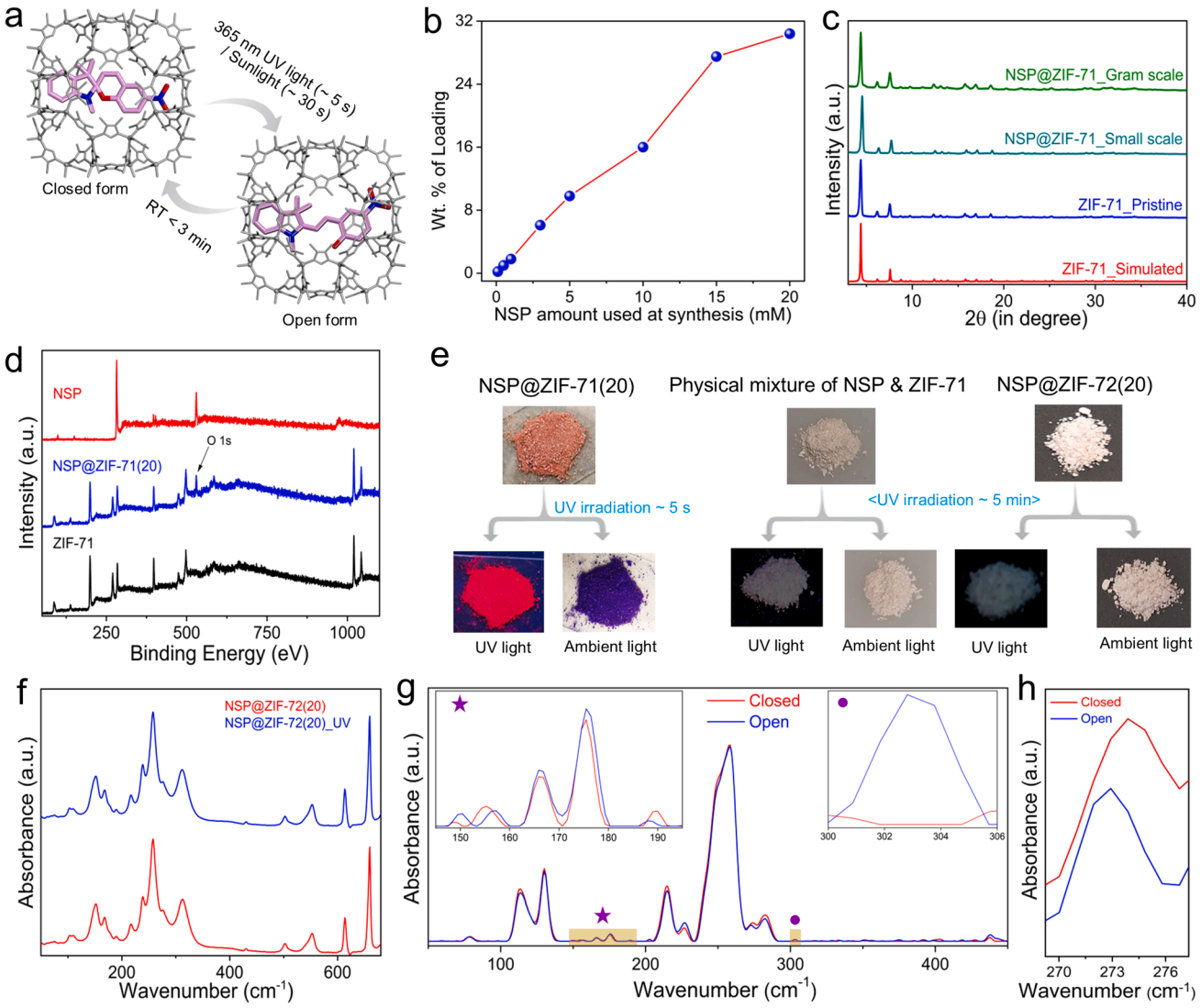

Fig. 2. Powder sample characterizations of the NSP@ZIF-71(20) nanocomposite. (a) Schematic diagrams and reversible color switching of the open ⇌ closed forms of the solid state photochromic material. 365 nm UV light was used for the color switching. (b) Different loading (wt.%) of NSP into the ZIF-71 host matrix. (c) PXRD patterns of ZIF-71 and composites, derived from the small- (~50 mg) and gram-scale (~4 g) production of NSP@ZIF-71(20). (d) XPS survey spectra of ZIF-71, NSP@ZIF-71(20) and NSP. (e) Photographs of NSP@ZIF-71(20), physical mixing of the NSP and ZIF-71, and NSP@ZIF-72(20). The NSP@ZIF-71(20) irradiated with UV light for 5 s while physical mixture and NSP@ZIF-72(20) both were irradiated for 5 min. No distinct color change was observed in both ambient light and under UV for the physical mixture and the NSP@ZIF-72(20) composite. (f) Far-infrared (farIR) spectra of NSP@ZIF-72(20) before and after UV irradiation. (g) Synchrotron-radiation far-infrared (SR-FIR) vibrational spectra for the open and closed form of NSP@ZIF-71(20); insets show a magnified view of the highlighted regions. (h) An enlarged view of Fig. 2e showing a peak shift at the strongest absorption band due to photochromic switching.

by MAF-6 and ZIF-11 (Table S1). When the pore of the host displays hydrophilic characteristics, the open configuration (polar) of the NSP is stabilized within the frameworks as a result of hydrophilic-hydrophilic interactions [49]. Therefore, achieving the optimal level of hydrophobicity is crucial for the effective performance of reversible photoisomerization (Scheme S1). The distinctive characteristics of ZIF-71 frameworks result in enhanced photochromic properties upon exposure to sunlight, surpassing those of other photochromic materials derived from MOFs. Furthermore, MOFs with electron-deficient pore surfaces such as ZIF-65, ZIF-68 and ZIF-70 are not conducive to photochromism generated by sunshine (Fig. 1 and Scheme S1). This is despite the fact that, the pore size of ZIF-70 is relatively larger than the size of the opened form of NSP molecules.

Fig. 2a shows the behavior of an efficient photochromic composite comprising the ZIF-71 host matrix, which has an ideal cage size and intermediate hydrophobicity to enable fast and reversible color switching of NSP upon UV irradiation or sunlight exposure (Fig. S8); the latter requires a greater sensitivity photochromic material. A maximum loading of 30.4 wt% of NSP confined in ZIF-71 has been achieved for the nanocomposite termed NSP@ZIF-71(20) (denoting 20 mM NSP guest used during synthesis of the composite), revealed by ^{1}H nuclear magnetic resonance (NMR) spectroscopy (see Fig. 2b, Figs. S9–S11 and Table S2). The NMR study determined that a solitary NSP molecule is enclosed within a mere 13.2 cages of the ZIF-71 framework in NSP@ZIF-71(20) composites. As expected, this number further increases for other composites with a lower guest loading, as shown in Table S2. Notably, gram-scale production of NSP@ZIF-71(20) has been achieved in a facile single-step reaction protocol at room temperature: such scalability is crucial for commercial and industrial applications (Fig. 2c). The XRD patterns of the composites matched the pristine MOF structure, indicating the formation of a highly crystalline phase (Fig. 2c). Raman scattering and Fourier transform infrared (FTIR) measurements were performed to determine the local microenvironment of the composites (Figs. S12–S16). The existence of the characteristic Raman peak for NSP at 1577 cm^{-1} in the composite confirms that NSP is embedded within the microenvironment of the ZIF-71 matrix (Fig. S12). The characteristic FTIR vibrational bands corresponding to NSP appear at 748.6 cm^{-1} and 1383.1 cm^{-1}, revealing encapsulation of NSP inside the ZIF-71 host matrix (Figs. S13–S16). Further, to gain detailed surface chemical composition of the composite, X-ray photoelectron spectroscopy (XPS) measurements were performed. Fig. 2d shows the appearance of a new O1s signal in the XPS spectra, which can be assigned to the NSP molecules in the composite material. The morphological features of the materials were examined by scanning electron microscopy (SEM) and atomic force microscopy (AFM), see Figs. S17–S18. Depending upon the reaction conditions used, either faceted micron-sized crystals (*ca.* 1–2 μm) or small nanocrystals (*ca.* 50 nm) may be obtained. Several controlled experiments were performed to determine the precise location of the NSP guest within the ZIF-71 frameworks, specifically to determine whether it was situated on the outer surface or within the pores (Figs. S19 and S20). The physical mixture of NSP and ZIF-71 powders, used as a control sample, did not exhibit color change when subjected to UV irradiation, as depicted in Fig. 2e. The outcome of this study provides indirect evidence that the NSP molecules do not exist on the outer surface of the NSP@ZIF-71(20) frameworks. No photoisomerization was observed in the photochromic composite after transformation of porous ZIF-71 (NSP@ZIF-71) to its nonporous ZIF-72 (NSP@ZIF-72) analogue, thereby validating the indispensability of the pore within the host MOF framework for the facile isomerization of NSP (Fig. 2e,f) [50].

To correlate the (bulk) powder phase photoisomerization process, we conducted density functional theory (DFT) calculations of NSP molecules and compared the high-resolution synchrotron far-infrared (FIR) vibrational spectra of nanocomposites (Fig. 2g,h and Figs. S21–S23, Table S3). The shifting of the terahertz (THz) collective modes of NSP@ZIF-71(20) below 200 cm^{-1} (<6 THz) upon ring opening of the NSP guests revealed the dynamic nature of the host matrix (inset Fig. 2g) [51]. Of note, a new characteristic vibrational band appears at 303.1 cm^{-1} (~10 THz) due to the opened configuration of the NSP molecules, while the existing vibrational band at 273.9 cm^{-1} (8.21 THz) of the ZIF-71 framework is red-shifted to 272.8 cm^{-1} (8.18 THz) due to the strong interaction between the host framework and the polar opened form of the NSP guest (Fig. 2h). The experimental determination of new vibrational bands at 202.5 cm^{-1}, 445 cm^{-1}, and 501 cm^{-1} after UV illumination is further evidence of the opened-ring merocyanine form of the NSP guests (Fig. S21). All the characteristics vibrational bands are assigned in Table S3.

2.2. Photoswitching of nano-sized crystalline particles

Near-field infrared nanospectroscopy (nanoFTIR) technique was employed for the first time as a local probe to interrogate the photoisomerization of nano-sized crystalline particles of NSP@ZIF-71(20) (Fig. 3a, Figs. S24–S27).

Here, nanoFTIR and scattering-type scanning near-field optical microscopy (s-SNOM) imaging provided us with the unique opportunity to chemically pinpoint the host–guest interaction and reversible photoisomerization process of the photochromic NSP molecules at the nanoscale (20 nm probing region) within the sub-micron crystal of the composite where even single crystal instrument fails [52]. The obtained s-SNOM optical phase images (Fig. S24) revealed that NSP is homogeneously distributed throughout the ZIF-71 crystals, without agglomeration of the guests on the surface [53]. Upon UV irradiation of NSP@ZIF-71(20), the nanoFTIR spectra show the appearance of three new vibrational bands at 1391 cm^{-1}, 1607 cm^{-1} and 1672 cm^{-1}, while the intensity of the vibrational peaks at 1105 cm^{-1}, 1638 cm^{-1} and 1662 cm^{-1} decreased due to a transformation of the closed-form of NSP into an opened merocyanine form which is polar (Figs. S25–S27). The vibrational band at 1130 cm^{-1} splits into two distinct peaks at 1139 cm^{-1} and 1118 cm^{-1} upon UV exposure; an observation that is attributed to the collective bond vibration of the opened form, which was attained by cleaving off the oxygen-containing six-membered ring of the closed form (inset Fig. 3a).

UV–Vis diffused reflectance spectroscopy (DRS) revealed bathochromic shifts in the presence of 365 nm UV light or sunlight, and hypsochromic shifts occurring in the dark under ambient conditions (Figs. S28 and S29, Table S4) (14). The distinct visual color change was clearly noticed for the NSP@ZIF-71(20) powder within 5 s of UV illumination or after 30 s of sunlight exposure, before reverting back to its original color within ~ 2.6 min derived from the kinetics of fading (Fig. S26b) under ambient conditions (or within 5 s at 50 °C). This photoswitchable behavior indicates facile reversible photoisomerization of the NSP confined in the ZIF-71 cavity (Fig. 3b). The spectral analysis shown in Fig. 3b indicates a slight red shift, even in the absence of UV irradiation. This phenomenon can be attributed to the material's elevated light sensitivity, which persists even under ambient lighting condition. The solid-state composite demonstrates a higher rate of switching when compared to the pristine NSP in solution state, despite the latter being present in extremely low concentration (Fig. S30). This is because of the perfect balance of porosity and hydrophobicity (Fig. 1), as well as a low guest loading (Table S2) found in the ZIF-71 frameworks. Using fluorescence spectroscopy, the open and closed forms of the NSP@ZIF-71(20) nanocomposite were registered upon excitation at 365 nm and 530 nm, respectively, while these two forms remained in an equilibrium state (isosbestic point) upon excitation at 430 nm (Fig. 3c, Figs. S31–S36 and Table S5). The absolute photoluminescence quantum yield (QY) of all the photochromic materials decreases upon UV irradiation (Tables S6–S9). The NSP@ZIF-71(20) nanocomposite powder exhibits the fastest switching time (characterized from its coloration and fading response), compared with other photochromic nanocomposites synthesized in this work (Fig. 3d); these results demonstrate the general applicability of the selection rules we proposed in Fig. 1.

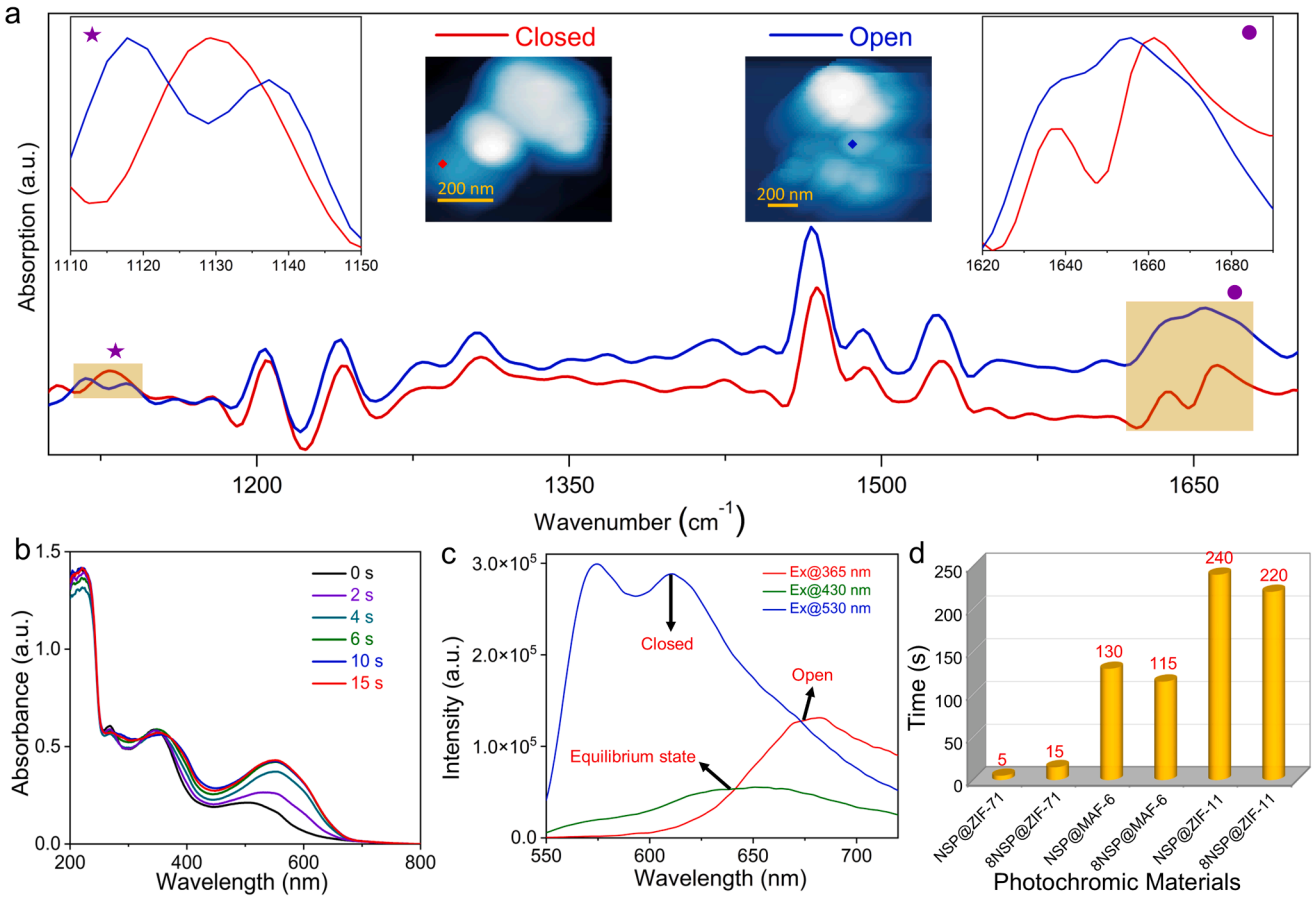

Fig. 3. Single crystal and optical characterizations of the photochromic materials. (a) Near-field nanoFTIR spectra of the closed and open forms of individual NSP@ZIF-71(20) nanocrystals at the designated locations (probe size < 20 nm) marked on the inset AFM images (red = before UV; blue = after UV irradiation). Inset graphs show the highlighted parts of the figure. (b) UV–Vis DRS of the NSP@ZIF-71(20) powder for different exposure times (0–15 s) subject to a 365-nm UV irradiation. (c) Emission spectra of the NSP@ZIF-71(20) powder at different excitation wavelengths. (d) A comparison of the photochromic transition times for various photochromic materials in powder form, each of which was synthesized using the same guest concentration of 20 mM. (For interpretation of the references to color in this figure legend, the reader is referred to the web version of this article.)

2.3. *Mechanically resilient photochromic films*

Pursuing real-world applications with these photochromic materials, detailed photochromic studies on thin films were carried out using a wide range of polymer matrices, such as PVDF (polyvinylidene difluoride), PDMS (polydimethyl siloxane), PS (polystyrene), PU (polyurethane), acrylate, and PMMA (polymethyl methacrylate) (Fig. 4. Figs. S37–S47). In this work, we have performed in-depth photochromic investigations of the NSP@ZIF-71(20)/PDMS and NSP@ZIF-71(20)/PS systems due to its merits in the form of transparent films, efficient photoswitching ability, and superior mechanical properties compared to the other polymer matrices being tested herein (Fig. S37). We fabricated several films with different loadings of photochromic material as a filler to yield various film thicknesses, ranging from 12 to 2000 μm utilizing the doctor-blade technique (Figs. S38–S43).

Remarkably, we established that a filler content as low as 1 wt% is already sufficient to achieve an intense visual color change in the presence of UV or natural sunlight (Figs. S39–S41). Transparency of the films was measured using transmission spectroscopy. Fig. S44 demonstrates that by increasing the thickness of the films, the transparency of the films decreases in comparison to the pristine PS films, despite the fact that the filler loading remained constant for each film. Upon UV irradiation, the characteristics of the merocyanine absorption maximum appear at 576 nm in UV–vis DRS (Fig. S45a), further confirming the open form of NSP molecules confined in the ZIF–71 host. Visual color switching was observed within 5 s upon UV irradiation (PDMS film), which will revert to its original state under ambient conditions within 120 s, as derived from the kinetics of color fading ($t_{1/2} \sim 51$ s) (Fig. S45). We found this color switching performance to be faster than the transition time required for the bulk powder samples (Fig. 4a). Of note, the photoswitching speed of both powders and film samples of the composites are much higher compared with the bare NSP-embedded films and solutions (see Fig. 4, Figs. S30 and S46). Significantly, the NSP@ZIF-71(20)/PDMS films exhibit one of the quickest reversible photoisomerization in contrast with existing reported photochromic materials based on porous materials and highest for MOF-based porous materials (Fig. 4b–c, Tables S10 and S11) [14,46,54–57]. Although a few photochromes exhibit fast reversible switching in films, their long-term stability and photostability remain unclear [58–61].

Production of high-quality photochromic films from MOF-based photochromic materials is another challenging task in the field. This issue can be resolved by employing a mechanically tough polymer matrix. However, the majority of the organic photoswitchable molecules do not exhibit photochromism after being combined with a mechanically "rigid" solid polymer (stiffness defined by the Young's modulus, E value of above 2 GPa) [14]. Nonetheless, mechanically resilient materials are essential for practical applications. We report for the first time that polymer matrices with a high mechanical stiffness (e.g., polystyrene (PS), $E \sim 4$ GPa) can also be engineered when the photochromic guest is encapsulated first inside the porous ZIF-71 cavity (Figs. S48). The mechanical properties of the photochromic films were further examined by the nanoindentation technique, so as to determine basic properties key

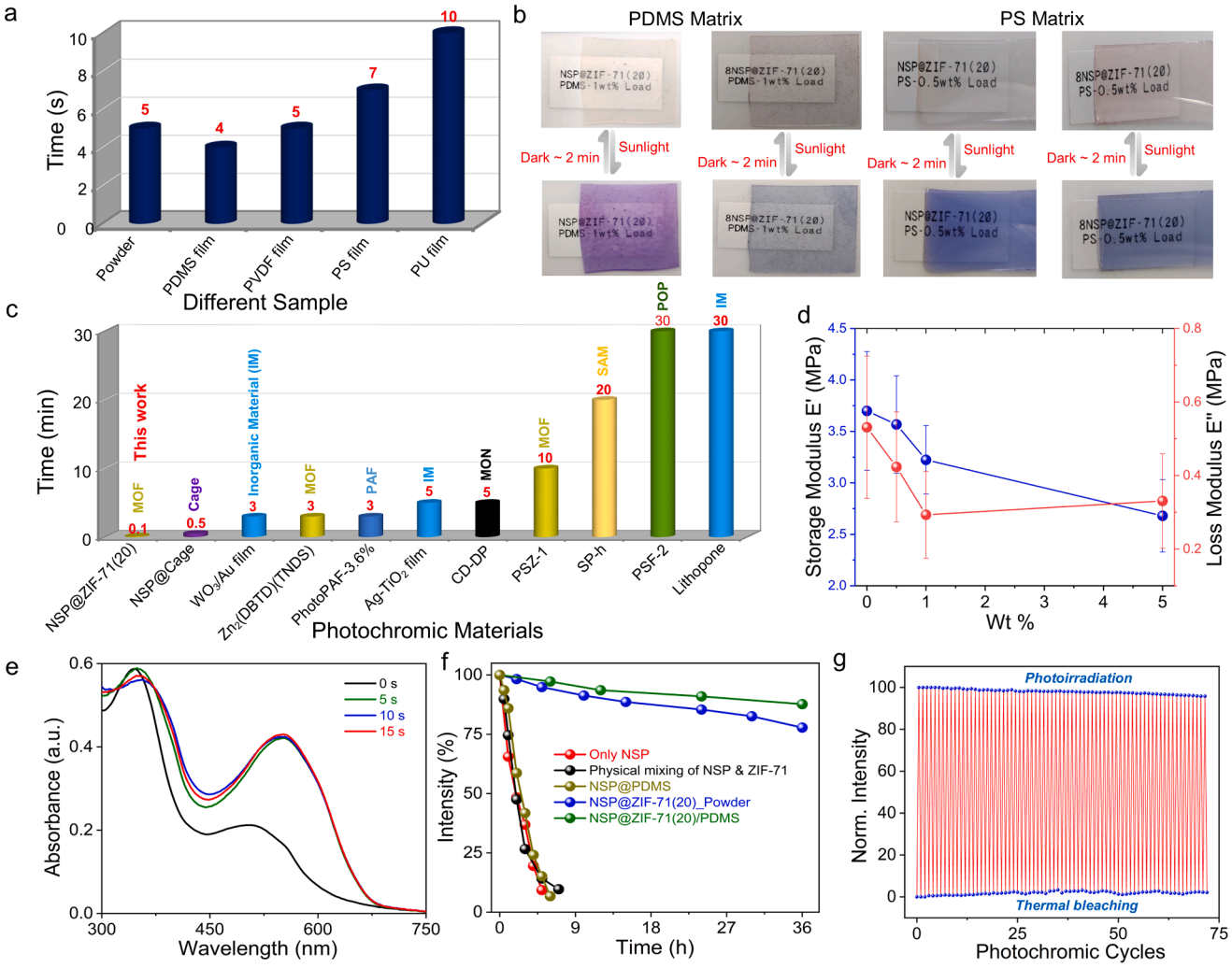

Fig. 4. Film characterization and photostability of photochromic materials. (a) Time taken for visual color change of the different photochromic nanocomposite films under 365 nm UV light. (b) Various thin films were fabricated by blending NSP@ZIF-71(20) and 8NSP@ZIF-71(20) with PDMS and PS polymer matrices, respectively. These films switch color in the presence of either 365 nm UV light (6 W lamp) or natural sunlight, where the nominal thickness of the film is *ca.* 190 μm. (c) A comparison of the transition times for photochromic switching of NSP@ZIF-71(20) versus other competing photochromic materials (see details in Table S8). (d) Probe-based dynamic mechanical analysis (nanoDMA) curves for the different loadings of NSP@ZIF-71(20) into PDMS films. (e) UV–Vis DRS of NSP@ZIF-71(20) powder subject to 0–15 s of 365 nm UV irradiation; samples tested after eight months of production. (f) Photostability tests for different photochromic materials. (g) Reversible photochromic cycles (72 cycles) showing the photo-induced fatigue resistance of the NSP@ZIF-71(20)/PDMS film.

to commercial thin films (Figs. S48 and S49). The flat punch and Berkovich indenters were used for the measurement of the mechanical properties of NSP@ZIF-71(20) incorporated into PDMS and PS polymer matrices, respectively. The elastic modulus (E) of the PS polymer decreases with an incremental amount of filler loading, where the stiffness value fell from 4.6 GPa (neat PS) to around 4.1 GPa at 15 wt% filler content (Fig. S48). This is a significant result because at present mechanically stiff polymers with $E > 2$ GPa will yield a poor photochromic response [14] (*vide infra*). In terms of the viscoelastic (time-dependent) mechanical response, the storage modulus (E') of the polymer matrix decreases with increasing amount of NSP@ZIF-71(20) filler, while the loss modulus (E'') initially decreases with the incremental amount of filler and reaches a minimum for 1 wt% (Fig. 4d). We hypothesise that the nanoparticles hindering crosslinking during PDMS curing may be the reason for the steady decline in storage modulus with higher filler addition. It is well-established that the crosslinking density of thermoset polymers directly relates to their mechanical stiffness [62]. On the other hand, the loss modulus measures the dissipation associated with viscous flow, which also decreases with filler loading (noting the larger uncertainties). There is a slight rise in loss modulus at 5 wt%, this corresponds to a higher loss tangent (Fig. S49) that may be attributed to frictional effect ascribed to particle aggregates. For the 1 wt% composite, the loss tangent values stay the lowest across all tested frequencies.

2.4. *Photo fatigue resistance*

Despite the success in the synthesis of various photochromic materials, the insufficient long-term stability, photobleaching, and the low recycling ability of organic photochromic materials are major barriers that seriously impede their potential in real-world applications. Although MOF-based photochromic materials are susceptible to low fatigue resistance, this effect is not well explored. Fig. 4e depicts the similar coloring rate as pristine materials over a period of several months, demonstrating the long-term environmental stability. Photobleaching tests were conducted by continuous exposure to an intense 365 nm UV light. Both the NSP@ZIF-71(20) powder and films have retained more than 75 % of their initial emission intensity even after 36 h of continuous exposure to high-intensity UV irradiation, while the bare NSP and physical mixing of the NSP and ZIF-71 samples rapidly degraded within 5 h (Fig. 4f, Fig. S50). To the best of our knowledge, this

is the first report concerning the photostability of NSP-MOF based photochromic materials. Furthermore, no detectable photodegradation was observed in the absorption intensity even after over 70 spontaneous colorations and fading cycles for the photochromic films (Fig. 4 g, Figs. S51–S52), validating the high photostability and robustness of the composite materials to photo-induced fatigue (Fig. 4f). The thermal bleaching test were conducted at a temperature of 50 °C. In the composite materials, a protecting barrier around the NSP molecules is formed, which serves to safeguard the NSP molecules by shielding them from direct contact with external light, thereby diminishing the occurrence of photobleaching. Furthermore, MOF serves to restrict their exposure to oxygen and the subsequent generation of reactive oxygen species during photochemical reactions, thereby augmenting their resistance to photo fatigue and prolonging the photostability of the molecules. It is noteworthy to mention that, our materials significantly outperform other photochromic materials comprising all types of porous frameworks including MOFs, COFs and cage in terms of the highly reversible photoswitching performance, unprecedented photo fatigue resistance and long-term stability, rendering the NSP@ZIF-71 material a strong contender for deployment in commercial and industrial settings [46].

2.5. Real-world applications

A variety of well-defined smooth and crack-free prototype photochromic sculptures were successfully fabricated by blending 1 wt% of NSP@ZIF-71(20) into a PDMS or PS polymer matrix to imitate the production of commercially viable photochromic components (Fig. 5 and Figs. S53–S55). The solid sculptures visually switch color within 5 s and 30 s upon irradiation by 365 nm UV light and sunlight, respectively. Subsequently, these materials could revert to their original color in the dark within 3 min at room temperature (Fig. 5a), and this transformation time is as good as commercial-grade inorganic photochromic materials [14]. In this work, a prototype of a large optically clear photochromic window and rewritable device were fabricated by blending 1 wt% of NSP@ZIF-71(20) with the PS polymer. The photochromic window changes color instantly when exposed to natural sunlight for a few seconds and will return to its original color in less than a minute in darkness (Fig. 5b, Movie S1). In another exemplar case, by illuminating a collimated 365-nm laser pointer on the rewritable device (see Movie S2), this instantly generates high-contrast handwriting or drawings that are swiftly erasable within minutes. Additionally, the devices made from the PS films are readily re-dissolved and recycled, which may reduce polymer waste and expand the life cycle of

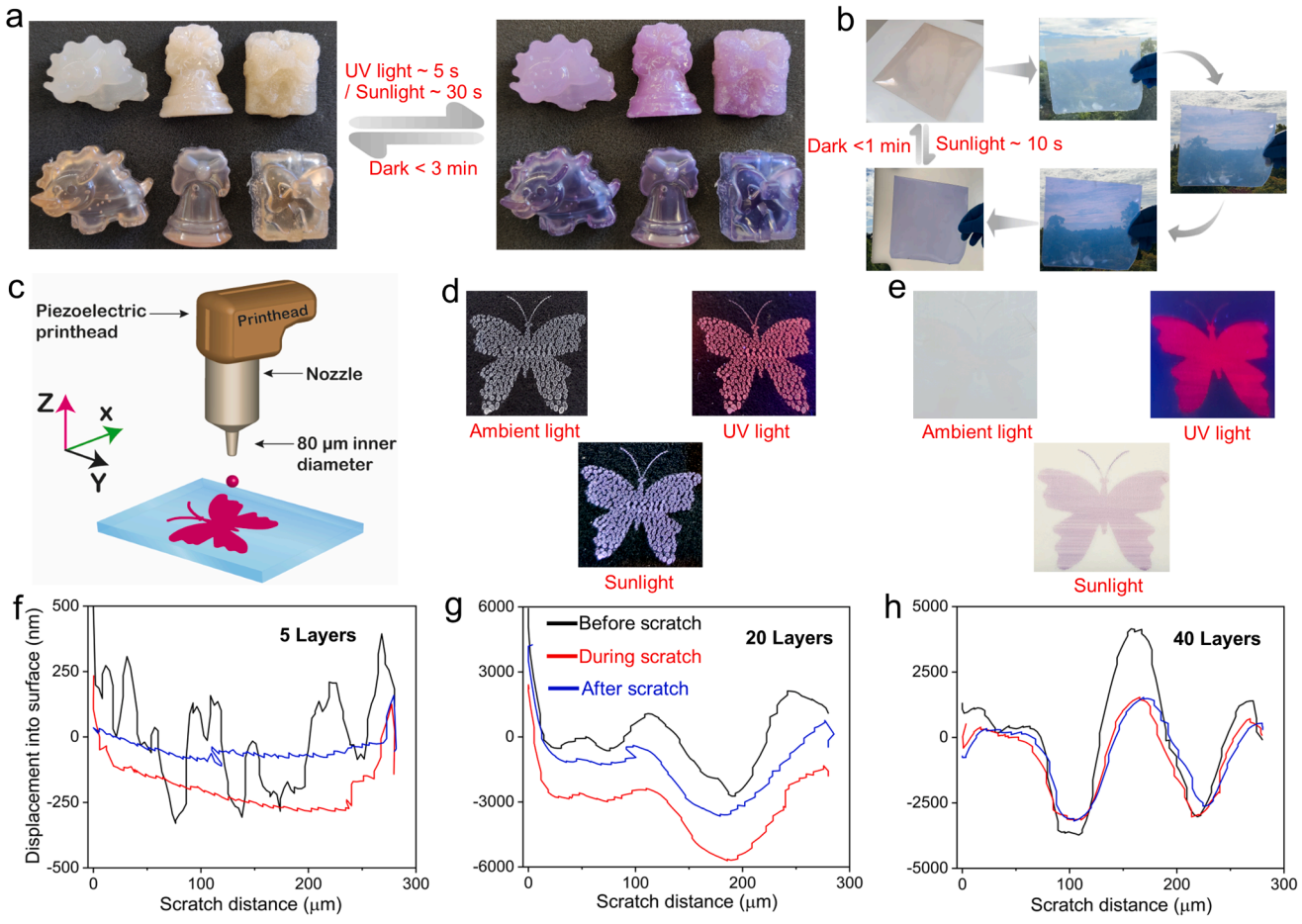

Fig. 5. Fabrication of different photochromic sculptures, transparent window, and emblems using the NSP@ZIF-71(20) nanocomposite. (a) Various photochromic sculptures were fabricated by blending 1 wt% of NSP@ZIF-71(20) with PDMS (top) and PS (bottom) polymer matrices. These sculptures readily switch their color in the presence of either 365 nm UV light or natural sunlight. (b) 20 × 15 cm^2 NSP@ZIF-71(20)/PS based photochromic window with a nominal thickness of *ca.* 350 μm. (c) An illustration of the inkjet printing technique. (d) Photographs of 2 layers of a butterfly image printed on a glass substrate. (e) Photographs of 2 layers of butterfly image printed on a PET substrate. When exposed to UV and sunlight, the printed image on both the glass and PET substrates changes color within just 5–10 s. Displacement and scratch distance data from a 1 mN nanoscratch ramp-load test by the plough mode over a scratch distance of 200 μm, on (f) 5 layers, (g) 20 layers, and (h) 40 layers of inkjet-printed NSP@ZIF-71(20) film on a glass substrate. Black, red, and blue traces corresponding to the initial surface scan, linear ramp scratch, and residual profile scan after tip unloading, respectively. (For interpretation of the references to color in this figure legend, the reader is referred to the web version of this article.)

engineered components.

Finally, piezoelectric-driven drop-on-demand inkjet printing was used for the precision coating of the bare nanocomposite materials on different substrates to create prototype photoswitchable printed films (Fig. 5c-e and Figs. S56–S72, see SI for details of the deposition method) [63]. The photochromic nanocomposites were homogeneously printed on a wide range of engineering substrates, such as silicon wafer, indium tin oxide (ITO)-coated flexible acetate sheets, glass substrates, PET substrates, and ITO-coated glass substrates, ranging from 50 nm to 2 μm in film thickness (Figs. S57–S74). AFM characterization revealed that the thickness of each layer of bare NSP@ZIF-71(20) film was around 30–50 nm, which is in good agreement with the height of each nanocrystal of the composites (Figs. S17, S63–S66). Fig. 5d and 5e demonstrates the 2-layer thickness of a butterfly emblem inkjet-printed on glass and PET substrates, respectively, showing their ability to spontaneously switch color subject to either UV irradiation or sunlight (Figs. S67–S69). The printed photochromic film is invisible when viewed against the white PET substrate in ambient light, but it becomes visible promptly under UV/sunlight, demonstrating its potential use in anticounterfeiting technology (Fig. 5e, Figs. S70–71). The materials adhesion to the substrate is a crucial parameter for commercial applications, and it was investigated for the first time for any photochromic materials based on porous frameworks, in these inkjet-printed samples on a glass substrate by systematic nanoscratch experiments accompanied by topographic characterizations (Fig. 5f-h, Figs. S73–S74, see the characterizations and physical measurements section in SI for more details) [64].

The scratch test revealed that as the inkjet-printed film thickness increases, the roughness of the film decreases while the material cohesion interaction is improved (Figs. S73–S74). In the scratch test for the 5-layer film, the indenter has already reached the substrate and the elastic recovery is attributed to the substrate; while for 40 layers, there is no elastic recovery because the indenter has just scratched the surface of the films (Fig. S73). Additionally, we also observed that chipping is the failure mechanism, and this is related to the cohesion of the nanocrystals of the photochromic materials (Fig. S74). The results suggest there is scope to tailor the mechanical resilience of the photochromic films and its fracture toughness by tuning the number of printed layers and thus modifying the film-to-substrate interactions for specific applications.

3. Conclusions

In summary, we have developed a set of easy-to-implement material selection rules, never before established in the porous materials domain including MOFs, for designing and engineering high-performance porous photochromic solids. Structural, optical, chemical, and mechanical characterizations have been systematically performed using a suite of multimodal techniques to elucidate the detailed behavior of the newly developed photochromic materials, from bulk powders to single crystals, and from polymer membranes to nanocrystalline thin films. Resilient solid-state photoswitchable materials have been fabricated and comprehensively studied, which have outperformed other NSP-based photochromic materials incorporating porous frameworks (e.g., MOFs, COFs, cages) in terms of their reversible photoswitching performance, photo fatigue resistance and long-term stability. Paving the way for advanced optical technologies, we have demonstrated the production of 3 D sculptures with complex geometries, smart window panels, and self-erasing rewritable screens by straightforward blending of mechanically stiff polymers (e.g., polystyrene) with NSP@MOF composite materials. Piezoelectric-driven drop-on-demand ink-jet printing was also shown for the first time to build MOF-based photochromic applications, by fabricating nanostructured films on a range of technical substrates for potential deployment in anticounterfeiting technology.

Declaration of Competing Interest

The authors declare that they have no known competing financial interests or personal relationships that could have appeared to influence the work reported in this paper.

Data availability

Data will be made available on request.

Acknowledgements

S.M., M.T., A.F.M., V.K. and J.C.T. thank the ERC consolidator Grant PROMOFS (grant agreement 771575) for funding the research. J.C.T. acknowledges the EPSRC IAA award (EP/R511742/1) for additional support. W.K. acknowledges the financial support provided by the Punjab Education Endowment Fund (PEEF), Pakistan. A.F.M. thanks the Oxford Ashton Memorial Scholarship for a D.Phil. studentship award. A. A.C-P was supported by The Royal Society through a University Research Fellowship (URF\R\180016) and the John Fell Fund, Oxford University Press, via a Pump-Priming grant (0005176). We acknowledge the Diamond Light Source (Harwell, Oxford) for the award of beamtime SM25407; we thank Dr Mark Frogley and Dr Gianfelice Cinque for their assistance during the B22 MIRIAM beamline. We thank the Research Complex at Harwell (RCaH) for the provision of materials characterization facilities. We thank Dr Sudarshan Narayan (Oxford Materials) for the XPS measurements.

Appendix A. Supplementary data

Supplementary data to this article can be found online at https://doi.org/10.1016/j.cej.2023.146727.

References

[1] W.R. Browne, B.L. Feringa, Making molecular machines work, Nat. Nanotechnol. 1 (1) (2006) 25–35.
[2] K. Kinbara, T. Aida, Toward intelligent molecular machines: directed motions of biological and artificial molecules and assemblies, Chem. Rev. 105 (4) (2005) 1377–1400.
[3] E.R. Kay, D.A. Leigh, F. Zerbetto, Synthetic molecular motors and mechanical machines, Angew. Chem. Int. Ed. 46 (1–2) (2007) 72–191.
[4] W.S. Wang, N. Xie, L. He, Y.D. Yin, Photocatalytic colour switching of redox dyes for ink-free light-printable rewritable paper, Nat. Commun. 5 (2014) 5459.
[5] T. Zhang, L. Sheng, J.N. Liu, L. Ju, J.H. Li, Z. Du, W.R. Zhang, M.J. Li, S.X.A. Zhang, Photoinduced proton transfer between photoacid and ph-sensitive dyes: influence factors and application for visible-light-responsive rewritable paper, Adv. Funct. Mater. 28 (16) (2018) 1705532.
[6] Z. Du, T. Zhang, H. Gai, L. Sheng, Y. Guan, X. Wang, T. Qin, M. Li, S. Wang, Y. M. Zhang, H. Nie, S.X. Zhang, Multi-component collaborative step-by-step coloring strategy to achieve high-performance light-responsive color-switching, Adv. Sci. 9 (2) (2022) e2103309.
[7] D. Han, B.L. Jiang, J. Feng, Y.D. Yin, W.S. Wang, Photocatalytic self-doped SnO2-x nanocrystals drive visible-light-responsive color switching, Angew. Chem. Int. Ed. 56 (27) (2017) 7792–7796.
[8] L. Wang, Q. Li, Photochromism into nanosystems: towards lighting up the future nanoworld, Chem. Soc. Rev. 47 (3) (2018) 1044–1097.
[9] Y. Yokoyama, Fulgides for memories and switches, Chem. Rev. 100 (5) (2000) 1717–1740.
[10] Z.Q. Li, G.N. Wang, Y.X. Ye, B. Li, H.R. Li, B.L. Chen, Loading photochromic molecules into a luminescent metal-organic framework for information anticounterfeiting, Angew. Chem. Int. Ed. 58 (50) (2019) 18025–18031.
[11] Y.H. Jin, Y.H. Hu, Y.R. Fu, L. Chen, G.F. Ju, Z.F. Mu, Reversible colorless-cyan photochromism in Eu2+-doped Sr3YNa(PO4)(3)F powders, J. Mater. Chem. B 3 (36) (2015) 9435–9443.
[12] Y.H. Jin, Y. Lv, C.L. Wang, G.F. Ju, H.Y. Wu, Y.H. Hu, Design and control of the coloration degree for photochromic Sr3GdNa(PO4)(3)F:Eu2+ via traps modulation by Ln3+ (Ln=Y, La-Sm, Tb-Lu) co-doping, Sens. Actuator B-Chem. 245 (2017) 256–262.
[13] Corning Incorporated, Photochromism Glass https://www.corning.com/worldwide/en/products/advanced-optics/product-materials/specialty-glass-and-glass-ceramics/ophthalmic-glass/photochromism.html. Date accessed September 2022. https://www.corning.com/worldwide/en/products/advanced-optics/product-materials/specialty-glass-and-glass-ceramics/ophthalmic-glass/photochromism.html. https://www.corning.com/worldwide/en/products/advanced-optics/product-materials/specialty-glass-and-glass-ceramics/ophthalmic-glass/photochromism.html.
[14] S.N. Corns, S.M. Partington, A.D. Towns, Industrial organic photochromic dyes, Color. Technol. 125 (5) (2009) 249–261.

[15] R. Klajn, Spiropyran-based dynamic materials, Chem. Soc. Rev. 43 (1) (2014) 148–184.
[16] L. Kortekaas, W.R. Browne, The evolution of spiropyran: fundamentals and progress of an extraordinarily versatile photochrome, Chem. Soc. Rev. 48 (12) (2019) 3406–3424.
[17] A.M. Rice, C.R. Martin, V.A. Galitskiy, A.A. Berseneva, G.A. Leith, N.B. Shustova, Photophysics modulation in photoswitchable metal-organic frameworks, Chem. Rev. 120 (16) (2020) 8790–8813.
[18] G.C. Thaggard, J. Haimerl, K.C. Park, J. Lim, R.A. Fischer, B.K.P. Maldeni Kankanamalage, B.J. Yarbrough, G.R. Wilson, N.B. Shustova, Metal-photoswitch friendship: from photochromic complexes to functional materials, J. Am. Chem. Soc. 144 (51) (2022) 23249–23263.
[19] C. Li, Y.G. Xue, M.D. Han, L.C. Palmer, J.A. Rogers, Y.G. Huang, S.I. Stupp, Synergistic photoactuation of bilayered spiropyran hydrogels for predictable origami-like shape change, Matter 4 (4) (2021) 1377–1390.
[20] C. Li, A. Iscen, L.C. Palmer, G.C. Schatz, S.I. Stupp, Light-driven expansion of spiropyran hydrogels, J. Am. Chem. Soc. 142 (18) (2020) 8447–8453.
[21] V.I. Minkin, Photo-, thermo-, solvato-, and electrochromic spiroheterocyclic compounds, Chem. Rev. 104 (5) (2004) 2751–2776.
[22] Y. Kobayashi, K. Mutoh, J. Abe, Fast photochromic molecules toward realization of photosynergetic effects, J. Phys. Chem. Lett. 7 (18) (2016) 3666–3675.
[23] H. Sato, R. Matsuda, K. Sugimoto, M. Takata, S. Kitagawa, Photoactivation of a nanoporous crystal for on-demand guest trapping and conversion, Nat. Mater. 9 (8) (2010) 661–666.
[24] Y.T. Zheng, H. Sato, P.Y. Wu, H.J. Jeon, R. Matsuda, S. Kitagawa, Flexible interlocked porous frameworks allow quantitative photoisomerization in a crystalline solid, Nat. Commun. 8 (2017) 100.
[25] S. Castellanos, F. Kapteijn, J. Gascon, Photoswitchable metal organic frameworks: turn on the lights and close the windows, CrstEngComm 18 (22) (2016) 4006–4012.
[26] D. Samanta, D. Galaktionova, J. Gemen, L.J.W. Shimon, Y. Diskin-Posner, L. Avram, P. Kral, R. Klajn, Reversible chromism of spiropyran in the cavity of a flexible coordination cage, Nat. Commun. 9 (2018) 641.
[27] H.A. Schwartz, U. Ruschewitz, L. Heinke, Smart nanoporous metal-organic frameworks by embedding photochromic molecules - state of the art and future perspectives, Photochem. Photobiol. Sci. 17 (7) (2018) 864–873.
[28] P.K. Kundu, G.L. Olsen, V. Kiss, R. Klajn, Nanoporous frameworks exhibiting multiple stimuli responsiveness, Nat. Commun. 5 (2014) 3588.
[29] M. Canton, A.B. Grommet, L. Pesce, J. Gemen, S.M. Li, Y. Diskin-Posner, A. Credi, G.M. Pavan, J. Andreasson, R. Klajn, Improving fatigue resistance of dihydropyrene by encapsulation within a coordination cage, J. Am. Chem. Soc. 142 (34) (2020) 14557–14565.
[30] J.H. Wang, L. Avram, Y. Diskin-Posner, M.J. Bialek, W. Stawski, M. Feller, R. Klajn, Altering the properties of spiropyran switches using coordination cages with different symmetries, J. Am. Chem. Soc. 144 (46) (2022) 21244–21254.
[31] Z.L. Chu, R. Klajn, Polysilsesquioxane nanowire networks as an “artificial solvent” for reversible operation of photochromic molecules, Nano Lett. 19 (10) (2019) 7106–7111.
[32] D. Samanta, J. Gemen, Z.L. Chu, Y. Diskin-Posner, L.J.W. Shimon, R. Klajn, Reversible photoswitching of encapsulated azobenzenes in water, PNAS 115 (38) (2018) 9379–9384.
[33] F. Castiglioni, W. Danowski, J. Perego, F.K. Leung, P. Sozzani, S. Bracco, S. J. Wezenberg, A. Comotti, B.L. Feringa, Modulation of porosity in a solid material enabled by bulk photoisomerization of an overcrowded alkene, Nat. Chem. 12 (7) (2020) 595–602.
[34] R. Haldar, L. Heinke, C. Woll, Advanced photoresponsive materials using the metal-organic framework approach, Adv. Mater. 32 (20) (2020) e1905227.
[35] W.P. Lustig, S. Mukherjee, N.D. Rudd, A.V. Desai, J. Li, S.K. Ghosh, Metal-organic frameworks: functional luminescent and photonic materials for sensing applications, Chem. Soc. Rev. 46 (11) (2017) 3242–3285.
[36] Z. Hu, Y. Wang, D. Zhao, The chemistry and applications of hafnium and cerium (iv) metal-organic frameworks, Chem. Soc. Rev. 50 (7) (2021) 4629–4683.
[37] I. Stassen, N. Burtch, A. Talin, P. Falcaro, M. Allendorf, R. Ameloot, An updated roadmap for the integration of metal-organic frameworks with electronic devices and chemical sensors, Chem. Soc. Rev. 46 (11) (2017) 3185–3241.
[38] J.D. Evans, V. Bon, I. Senkovska, H.C. Lee, S. Kaskel, Four-dimensional metal-organic frameworks, Nat. Commun. 11 (1) (2020) 2690.
[39] X. Han, S.H. Yang, M. Schroder, Porous metal-organic frameworks as emerging sorbents for clean air, Nat. Rev. Chem. 3 (2) (2019) 108–118.
[40] L.F. Lin, X. Han, B.X. Han, S.H. Yang, Emerging heterogeneous catalysts for biomass conversion: studies of the reaction mechanism, Chem. Soc. Rev. 50 (20) (2021) 11270–11292.
[41] E.A. Dolgopolova, V.A. Galitskiy, C.R. Martin, H.N. Gregory, B.J. Yarbrough, A. M. Rice, A.A. Berseneva, O.A. Ejegbavwo, K.S. Stephenson, P. Kittikhunnatham, S. G. Karakalos, M.D. Smith, A.B. Greytak, S. Garashchuk, N.B. Shustova, Connecting wires: photoinduced electronic structure modulation in metal-organic frameworks, J. Am. Chem. Soc. 141 (13) (2019) 5350–5358.
[42] K. Healey, W. Liang, P.D. Southon, T.L. Church, D.M. D'Alessandro, Photoresponsive spiropyran-functionalised MOF-808: postsynthetic incorporation and light dependent gas adsorption properties, J. Mater. Chem. A 4 (28) (2016) 10816–10819.
[43] S. Garg, H. Schwartz, M. Kozlowska, A.B. Kanj, K. Muller, W. Wenzel, U. Ruschewitz, L. Heinke, Conductance photoswitching of metal-organic frameworks with embedded spiropyran, Angew. Chem. Int. Ed. 58 (4) (2019) 1193–1197.
[44] K. Muller, J. Helfferich, F.L. Zhao, R. Verma, A.B. Kanj, V. Meded, D. Bleger, W. Wenzel, L. Heinke, Switching the proton conduction in nanoporous, crystalline materials by light, Adv. Mater. 30 (8) (2018) 1706551.
[45] M. Gutierrez, Y. Zhang, J.C. Tan, Confinement of luminescent guests in metal-organic frameworks: understanding pathways from synthesis and multimodal characterization to potential applications of LG@MOF systems, Chem. Rev. 122 (11) (2022) 10438–10483.
[46] J. Zhang, H. Tian, Industrial applications and perspectives, photochromic materials: preparation, properties and applications, Wiley-VCH Weinheim, Germany, 2016, pp. 393–415.
[47] T. Zhang, Z.F. Yang, J.X. Wang, L. Chen, C. Li, A metastable-state photoacid-based metal organic framework with multi-stimuli-responsive chromism, Dyes Pigm. 203 (2022), 110365.
[48] D.E. Williams, C.R. Martin, E.A. Dolgopolova, A. Swifton, D.C. Godfrey, O. A. Ejegbavwo, P.J. Pellechia, M.D. Smith, N.B. Shustova, Flipping the switch: fast photoisomerization in a confined environment, J. Am. Chem. Soc. 140 (24) (2018) 7611–7622.
[49] F. Zhang, X.Q. Zou, W. Feng, X.J. Zhao, X.F. Jing, F.X. Sun, H. Ren, G.S. Zhu, Microwave-assisted crystallization inclusion of spiropyran molecules in indium trimesate films with antidromic reversible photochromism, J. Mater. Chem. 22 (48) (2012) 25019–25026.
[50] M. Tu, D.E. Kravchenko, B.Z. Xia, V. Rubio-Gimenez, N. Wauteraerts, R. Verbeke, I. F.J. Vankelecom, T. Stassin, W. Egger, M. Dickmann, H. Amenitsch, R. Ameloot, Template-mediated control over polymorphism in the vapor-assisted formation of zeolitic imidazolate framework powders and films, Angew. Chem. Int. Ed. 60 (14) (2021) 7553–7558.
[51] A.F. Möslein, J.-C. Tan, Vibrational modes and terahertz phenomena of the large-cage zeolitic imidazolate framework-71, J. Phys. Chem. Lett. 13 (12) (2022) 2838–2844.
[52] A.F. Moslein, M. Gutierrez, B. Cohen, J.C. Tan, Near-field infrared nanospectroscopy reveals guest confinement in metal-organic framework single crystals, Nano Lett. 20 (10) (2020) 7446–7454.
[53] Y. Zhang, T. Xiong, A.F. Moslein, S. Mollick, V. Kachwal, A.S. Babal, N. Amin, J. C. Tan, Nanoconfinement of tetraphenylethylene in zeolitic metal-organic framework for turn-on mechanofluorochromic stress sensing, Appl. Mater. Today 27 (2022), 101434.
[54] A. Towns, Photochromic dyes, Phys. Sci. Rev. 6 (9) (2021) 477–511.
[55] M. Casini, Active dynamic windows for buildings: a review, Renew. Energy 119 (2018) 923–934.
[56] H.J. Hoffmann, The use of silver salts for photochromic-glasses, Photochromism 40 (1990) 822–854.
[57] R. Tallberg, B.P. Jelle, R. Loonen, T. Gao, M. Hamdy, Comparison of the energy saving potential of adaptive and controllable smart windows: a state-of-the-art review and simulation studies of thermochromic, photochromic and electrochromic technologies, Sol. Energy Mater. Sol. Cells 200 (2019), 109828.
[58] R.A. Evans, T.L. Hanley, M.A. Skidmore, T.P. Davis, G.K. Such, L.H. Yee, G.E. Ball, D.A. Lewis, The generic enhancement of photochromic dye switching speeds in a rigid polymer matrix, Nat. Mater. 4 (3) (2005) 249–253.
[59] H. Kuroiwa, Y. Inagaki, K. Mutoh, J. Abe, On-demand control of the photochromic properties of naphthopyrans, Adv. Mater. 31 (2) (2019).
[60] H. Torres-Pierna, D. Ruiz-Molina, C. Roscini, Highly transparent photochromic films with a tunable and fast solution-like response, Mater. Horizons 7 (10) (2020) 2749–2759.
[61] N. Vazquez-Mera, C. Roscini, J. Hernando, D. Ruiz-Molina, Liquid-filled capsules as fast responsive photochromic materials, Adv. Opt. Mater. 1 (9) (2013) 631–636.
[62] Z.X. Wang, A.A. Volinsky, N.D. Gallant, Crosslinking effect on polydimethylsiloxane elastic modulus measured by custom-built compression instrument, J. Appl. Polym. Sci. 131 (22) (2014).
[63] W. Kamal, M. Li, J.D. Lin, E. Parry, Y. Jin, S.J. Elston, A.A. Castrejón-Pita, S. M. Morris, Spatially patterned polymer dispersed liquid crystals for image-integrated smart windows, Adv. Opt. Mater. 10 (3) (2021) 2101748.
[64] I. Stassen, M. Styles, T. Van Assche, N. Campagnol, J. Fransaer, J. Denayer, J. C. Tan, P. Falcaro, D. De Vos, R. Ameloot, Electrochemical film deposition of the zirconium metal-organic framework UiO-66 and application in a miniaturized sorbent trap, Chem. Mater. 27 (5) (2015) 1801–1807.